

Mixed conductivity, oxygen permeability and redox behavior of K_2NiF_4 -type $La_2Ni_{0.9}Fe_{0.1}O_{4+\delta}$

V.V. Kharton^{a,*}, E.V. Tsipis^b, E.N. Naumovich^a, A. Thursfield^c, M.V. Patrakeev^d, V.A. Kolotygin^a, J.C. Waerenborgh^b, I.S. Metcalfe^c

^a Department of Ceramics and Glass Engineering, CICECO, University of Aveiro, 3810-193 Aveiro, Portugal

^b Chemistry Department, ITN/CFMC-UL, Estrada Nacional 10, P-2686-953 Sacavém, Portugal

^c School of Chemical Engineering and Advanced Materials, Newcastle University, Newcastle upon Tyne NE1 7RU, UK

^d Institute of Solid State Chemistry, UB RAS, 91 Pervomaiskaya Street, 620219 Ekaterinburg, Russian Federation

ARTICLE INFO

Article history:

Received 6 December 2007

Received in revised form

17 March 2008

Accepted 22 March 2008

Available online 26 March 2008

Keywords:

Lanthanum nickelate

Mixed conductivity

Oxygen permeability

Oxygen non-stoichiometry

Ceramic membrane

Methane oxidation

ABSTRACT

The total conductivity and Seebeck coefficient of $La_2Ni_{0.9}Fe_{0.1}O_{4+\delta}$ with K_2NiF_4 -type structure, studied in the oxygen partial pressure range from 10^{-5} to 0.5 atm at 973–1223 K, were analyzed in combination with the steady-state oxygen permeability, oxygen non-stoichiometry and Mössbauer spectroscopy data in order to examine the electronic and ionic transport mechanisms. Doping of $La_2NiO_{4+\delta}$ with iron was found to promote hole localization on nickel cations due to the formation of stable Fe^{3+} states, although the electrical properties dominated by p-type electronic conduction under oxidizing conditions exhibit trends typical for both itinerant and localized behavior of the electronic sublattice. The segregation of metallic Ni on reduction, which occurs at oxygen chemical potentials close to the low- $p(O_2)$ stability boundary of undoped lanthanum nickelate, is responsible for the high catalytic activity towards partial oxidation of methane by the lattice oxygen of $La_2Ni_{0.9}Fe_{0.1}O_{4+\delta}$ as revealed by thermogravimetry and temperature-programmed reduction in dry CH_4 -He flow at 573–1173 K. A model for the oxygen permeation fluxes through dense $La_2Ni_{0.9}Fe_{0.1}O_{4+\delta}$ ceramics, limited by both bulk ionic conduction and surface exchange kinetics, was proposed and validated.

© 2008 Elsevier Inc. All rights reserved.

1. Introduction

Mixed conductors derived from the rare-earth nickelates with K_2NiF_4 -type structure, $Ln_2NiO_{4+\delta}$ ($Ln = La, Pr, Nd$), have attracted much attention as promising materials for solid oxide fuel cell (SOFC) cathodes and ceramic membranes for oxygen separation and partial oxidation of light hydrocarbons [1–12]. Important advantages of Ln_2NiO_4 -based materials include substantially high oxygen permeability and ionic conductivity, moderate thermal and chemically induced expansion, and high electrocatalytic activity. The oxygen permeation through dense nickelate membranes is essentially limited by kinetics of surface redox processes [1,4,10], which prevents bulk decomposition and enables stable operation under air/ CH_4 gradients up to temperatures as high as 1173 K [12].

The crystal structure of $La_2NiO_{4+\delta}$ is built of alternating rock-salt La_2O_2 and perovskite NiO_2 layers, and can accommodate a significant oxygen excess [1–4,6–8,11,13–15]. The extra O^{2-} anions are charge-compensated by the p-type electronic charge carriers

and occupy interstitial positions in the LaO bilayers, while the concentration of oxygen vacancies in the perovskite sheets is very low. In air, the equilibrium oxygen hyperstoichiometry (δ) is close to 0.14–0.15 at 300 K and decreases on heating; the structure is tetragonal (space group $I4/mmm$ or $F4/mmm$) [3,6,15,16]. The orthorhombic $Fmmm$ and $Bmab$ lattices are formed on increasing and decreasing oxygen content, respectively [13,16]. Doping with higher-valence cations, such as iron, results in a higher concentration of interstitial anions and may have a favorable effect on the ionic transport [4,7]. The total conductivity of lanthanum nickelate and its analogs is predominantly p-type electronic [3,4,8–11]; the ionic contribution estimated from oxygen permeation data [4,10,12,17,18] is 10^2 – 10^4 times lower than the hole conduction.

The information available on defect formation and transport mechanisms relevant to the oxygen permeation and catalytic behavior of La_2NiO_4 -based phases is, however, scarce and often contradicting. For example, the catalytic performance of dense $La_2NiO_{4+\delta}$ membranes was found to be governed by partial reduction of the ceramic surface exposed to the reducing atmosphere and by the formation of a porous La_2O_3 -supported Ni catalyst layer which may act to provide high selectivity towards the partial oxidation of methane [5]. At the same time, the

* Corresponding author. Fax: +351 234 425300.

E-mail address: kharton@ua.pt (V.V. Kharton).

steady-state methane conversion over planar $\text{La}_2\text{Ni}_{0.9}\text{Co}_{0.1}\text{O}_{4+\delta}$ membranes and the pulse oxidation of dry CH_4 over powdered membrane material both lead to predominant total combustion [12,18]. The $p(\text{O}_2)$ - T - δ diagrams of $\text{La}_2(\text{Ni},\text{M})\text{O}_{4+\delta}$ ($M = \text{Fe}, \text{Co}, \text{Cu}$) can be adequately described by a statistical thermodynamic approach, accounting for the site-exclusion effects due to the coulombic repulsion of oxygen interstitials and interaction of holes localized on the Ni-site cations [11,15]; however, the variations of the partial electronic conductivity in $\text{La}_2\text{Ni}_{0.9}\text{Fe}_{0.1}\text{O}_{4+\delta}$ reveal a tendency for hole delocalization [11]. The latter may require use of another approach [19] based on the rigid-band approximation [20,21] for the description of oxygen intercalation and permeation processes.

Continuing our studies of Ln_2NiO_4 -based mixed conductors [4,10–12,15,18,22], the present work is centered on the analysis of oxygen permeability, electronic conductivity, Seebeck coefficient and catalytic behavior of $\text{La}_2\text{Ni}_{0.9}\text{Fe}_{0.1}\text{O}_{4+\delta}$ selected as a prototype membrane material. Particular attention is focused on the studies of ionic and electronic transport properties as a function of the oxygen partial pressure, and on the assessment of dry CH_4 oxidation over $\text{La}_2\text{Ni}_{0.9}\text{Fe}_{0.1}\text{O}_{4+\delta}$ by the temperature-programmed reduction (CH_4 -TPR) technique. The data on oxygen non-stoichiometry, used in this work for the calculations of equilibrium charge-carrier concentration and for modelling of the oxygen transport under non-equilibrium conditions, are reported elsewhere [11]. In order to clarify the electronic conduction mechanism, an attempt to analyze the $p(\text{O}_2)$ - T - δ diagrams using a rigid-band model [19] was undertaken in comparison with the site-exclusion approach [15]. Also, selected experimental and theoretical results are compared to the available data on $\text{La}_2\text{NiO}_{4+\delta}$ and $\text{La}_2\text{Ni}_{0.9}\text{Co}_{0.1}\text{O}_{4+\delta}$ [15,18,23] in order to evaluate effects of iron doping.

2. Experimental

Submicron powder of $\text{La}_2\text{Ni}_{0.9}\text{Fe}_{0.1}\text{O}_{4+\delta}$ was synthesized by the glycine-nitrate process [24] with subsequent annealing in air at 1073–1373 K for 2–5 h and ball-milling. Gas-tight ceramics having 95% density were sintered in air at 1593–1723 K during 2–10 h and cooled down to room temperature at $1\text{--}2\text{ K min}^{-1}$ to achieve equilibrium with atmospheric oxygen. The formation of single K_2NiF_4 -type phase and the overall cation composition were confirmed by X-ray diffraction (XRD) and inductively coupled plasma (ICP) spectroscopic analysis, respectively. The unit cell parameters of as-prepared $\text{La}_2\text{Ni}_{0.9}\text{Fe}_{0.1}\text{O}_{4+\delta}$, equilibrated in air at low temperatures, were determined as $a = 5.4884(2)\text{ \AA}$, $b = 5.4809(2)\text{ \AA}$ and $c = 12.6737(4)\text{ \AA}$ (S.G. *Fmmm*); the oxygen excess measured by thermogravimetric analysis (TGA) was 0.174 atoms per formula unit. The energy-dispersive spectroscopy (EDS) demonstrated an absence of compositional differences between the grains and grain-boundaries in $\text{La}_2\text{Ni}_{0.9}\text{Fe}_{0.1}\text{O}_{4+\delta}$ ceramics, within the limits of experimental uncertainty; the grain size evaluated by scanning electron microscopy (SEM), varied in the range 4–12 μm . Additional series of ceramic samples used for the analysis of phase composition at elevated temperatures, were annealed in various atmospheres and then quenched in liquid nitrogen. The Rietveld refinement results for $\text{La}_2\text{Ni}_{0.9}\text{Fe}_{0.1}\text{O}_{4+\delta}$ equilibrated in oxidizing and reducing conditions have been published previously [11].

The equipment and experimental procedures used for characterization, including XRD, SEM/EDS, TGA, coulometric titration (CT), dilatometry, and measurements of the total electrical conductivity (4-probe DC), Seebeck coefficient and steady-state oxygen permeation fluxes are described elsewhere [4,10–12, 15,18,22,23,25]. All data on oxygen permeability presented in this

work correspond to the membrane feed-side oxygen partial pressure (p_2) maintained at 0.21 atm (atmospheric air); the permeate-side oxygen partial pressure (p_1) varied in the range 6×10^{-3} to 0.20 atm. The isothermal measurements of the total conductivity (σ) and Seebeck coefficient (α) as functions of the oxygen partial pressure were performed at 973–1223 K in the $p(\text{O}_2)$ range from 0.5 down to 10^{-14} atm. Reproducibility of the electrical properties was checked independently for two pairs of ceramic samples, both studied under $p(\text{O}_2)$ cycling performed separately in oxidizing atmospheres and then in the whole $p(\text{O}_2)$ range. As illustrated by Fig. 1A, excellent agreement between the data obtained on redox cycling was observed under oxidizing conditions, at $p(\text{O}_2) > 10^{-5}$ atm. At lower $p(\text{O}_2)$ values when $\text{La}_2\text{Ni}_{0.9}\text{Fe}_{0.1}\text{O}_{4+\delta}$ remains single-phase, but its structure transforms from tetragonal to orthorhombic (S.G. *Bmab*) [11], significant hysteresis phenomena occur. In order to avoid possible uncertainties caused by stagnated gas diffusion at the oxygen partial pressures below 10^{-5} atm [26], the results on electrical properties presented in this work are limited to oxidizing environments only.

The temperature-programmed reduction (TPR) and oxidation (TPO) experiments were carried out using an automated CATLAB system (Hiden Analytical, UK) with one microreactor, feeding into a soft ionization mass spectrometer (QIC-20) via a heated

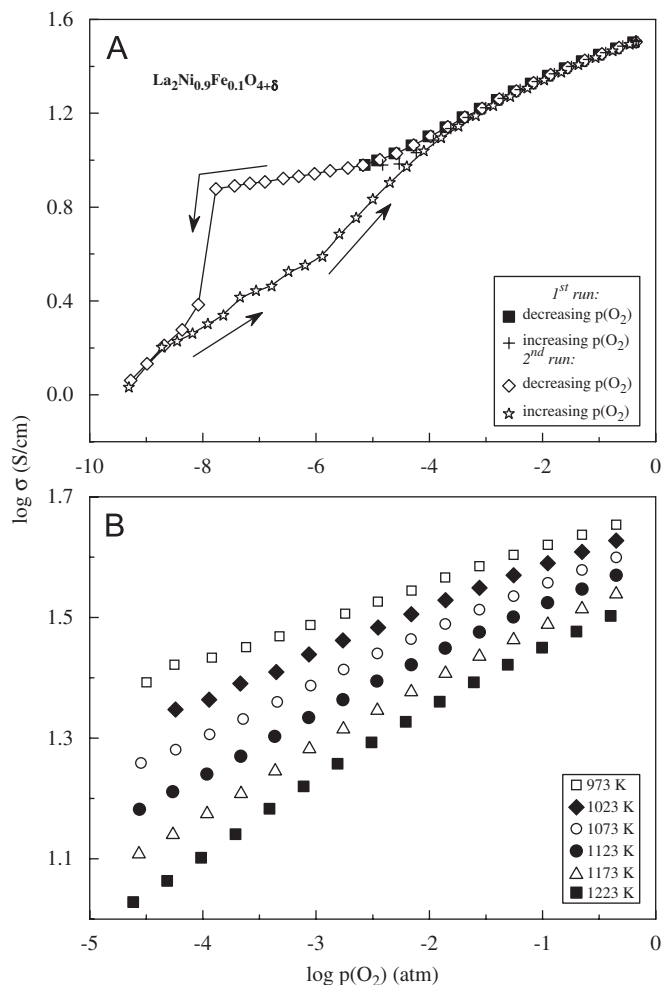


Fig. 1. Oxygen partial pressure dependencies of the total conductivity of $\text{La}_2\text{Ni}_{0.9}\text{Fe}_{0.1}\text{O}_{4+\delta}$. The data in (A) were obtained on redox cycling during two runs performed under oxidizing conditions and in the whole $p(\text{O}_2)$ range in order to check reproducibility of the electrical properties. Arrows indicate the directions of $p(\text{O}_2)$ changes.

capillary line for continuous online analysis. Spectral interference was taken into account between species and the mass 28 contributions from any N_2 leak into the system was minimized by leaving the system under constant helium flush. In the course of the CH_4 -TPR and TPO tests, the powdered sample (weight 50 mg, specific surface area $0.7\text{ m}^2\text{ g}^{-1}$) was placed in a quartz tube of small volume (0.1 cm^3) to facilitate fast response and negligible memory effects. The test sequence employed a heating step to 573 K at 10 K min^{-1} in helium. This was immediately followed by the TPR step: heating to 1173 K under 10% CH_4 –90% He (26.9 ml min^{-1} , STP) at 5, 10 or 20 K min^{-1} . Then the reactor was flushed with helium for 30 min and cooled either under 20% O_2 –80% He flow or under pure He atmosphere; the latter procedure was followed by the TPO experiments in which the sample was ramped to 1173 K under 20% O_2 –80% He and cooled in flowing helium. The reduction/oxidation cycles were repeated more than 10 times in order to validate reproducibility of the results.

3. Results and discussion

3.1. Hole conduction and Seebeck coefficient in oxidizing atmospheres

The electrical conductivity behavior of $La_2Ni_{0.9}Fe_{0.1}O_{4+\delta}$ under oxidizing conditions (Figs. 1B and 2) is similar to that of undoped $La_2NiO_{4+\delta}$ and its derivatives [3,4,6,8,15,27]. In air, the conductivity is thermally activated at temperatures below approximately 680 K; the corresponding activation energy, $9.8 \pm 0.2\text{ kJ mol}^{-1}$, is characteristic of a small-polaron mechanism [28]. At higher temperatures when progressive oxygen loss from the lattice begins, the behavior appears to become pseudometallic, primarily due to decreasing hole concentration on heating. In this regime, the substitution of 10% Fe or Co for Ni decreases the total conductivity, exhibiting an inverse correlation with the oxygen non-stoichiometry variations [11,15]. This validates the conclusion

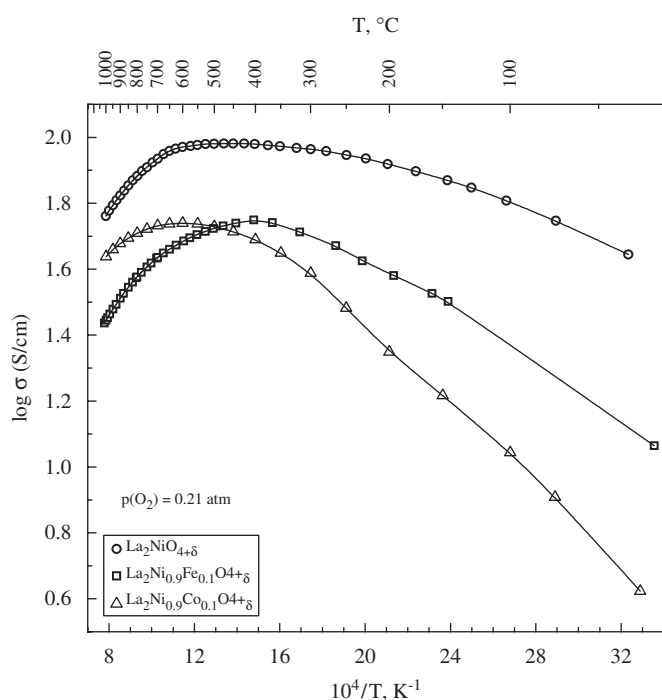


Fig. 2. Temperature dependencies of the total conductivity of La_2NiO_4 -based materials in air.

on hole trapping by iron and cobalt cations forming stable Fe^{3+} and Co^{3+} states, which was drawn based on statistical-thermodynamic modelling of the $p(O_2)$ – T – δ diagrams [11,15]. Indeed, the Mössbauer spectroscopy analysis of $La_2Ni_{0.9}Fe_{0.1}O_{4+\delta}$ indicated an absence of either Fe^{4+} or Fe^{2+} within the limits of experimental error [11]. Increasing oxygen excess in $La_2Ni_{0.9}Fe_{0.1}O_{4+\delta}$ above $\delta = 0.05$ should hence be charge-compensated by rising the nickel oxidation state from 2+ to 3+. As expected, reduction of the oxygen partial pressure down to 10^{-5} – 10^{-4} atm leads to lower conductivity, while the Seebeck coefficient increases and has positive sign (Figs. 1 and 3), thus indicating that electronic transport is dominated by p-type charge carriers.

Fig. 4 compares the partial ionic (σ_o) and p-type electronic (σ_h) conductivities, which were separated by analyzing the oxygen permeation data as discussed below. The ionic contribution to total conductivity increases with temperature, but oxygen ion transference numbers (t_o) do not exceed 0.02 at 1223 K. The electron–hole mobility (u_h , Fig. 4B) was calculated from the σ_h values and p-type charge carrier concentration estimated from the $p(O_2)$ – T – δ diagram of $La_2Ni_{0.9}Fe_{0.1}O_{4+\delta}$. The mobility is almost $p(O_2)$ -independent due to an essentially constant occupancy of the oxygen sites in the perovskite-type (Ni,Fe) O_2 layers [13–16] and to very low chemical expansion of the lanthanum nickelate lattice [11]. The tendency to a slight decrease on heating might indicate a substantial delocalization of p-type charge carriers. Notice that in the case of polaronic conduction, the mobility at

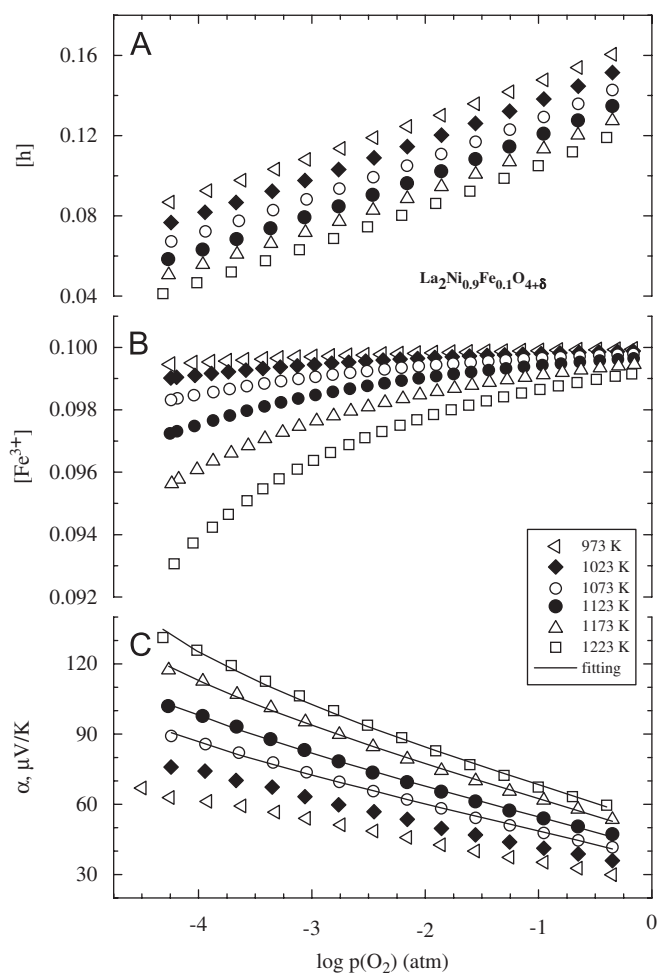


Fig. 3. Oxygen partial pressure dependencies of the relative concentrations of holes (A) and Fe^{3+} cations (B) calculated from the oxygen non-stoichiometry data, and Seebeck coefficient (C) of $La_2Ni_{0.9}Fe_{0.1}O_{4+\delta}$. Solid lines correspond to the fitting results using Eq. (1).

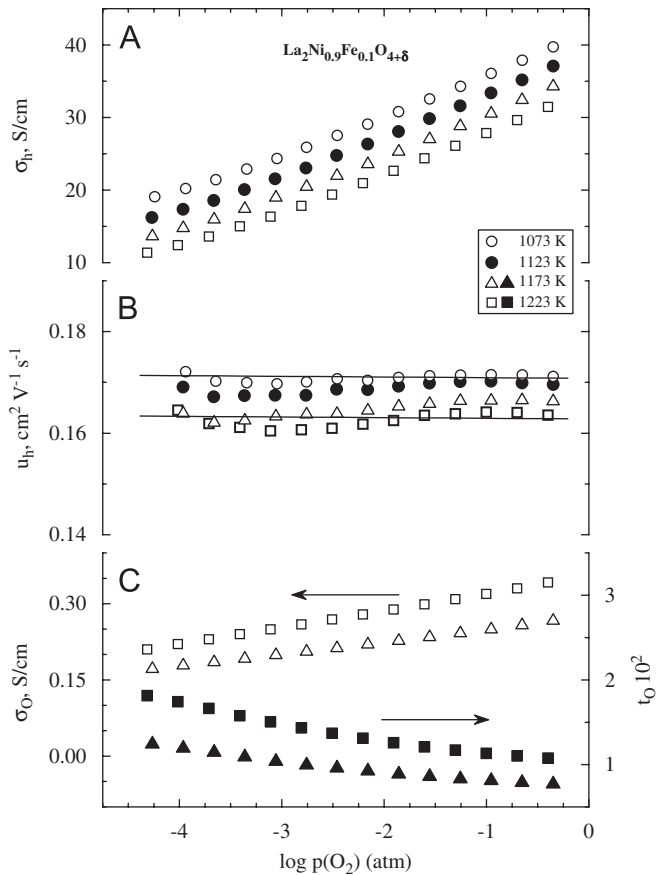


Fig. 4. Oxygen partial pressure dependencies of the partial p-type electronic conductivity (A), hole mobility (B), oxygen ionic conductivity and ion transference numbers (C) of $\text{La}_2\text{Ni}_{0.9}\text{Fe}_{0.1}\text{O}_{4+\delta}$ as calculated from the oxygen non-stoichiometry, total conductivity and oxygen permeability data (see text).

elevated temperatures is expected to be thermally activated and follow an Arrhenius model, with an activation energy of about 5–25 kJ mol^{-1} [28].

The Seebeck coefficient of $\text{La}_2\text{Ni}_{0.9}\text{Fe}_{0.1}\text{O}_{4+\delta}$ is relatively high and temperature-dependent (Fig. 3C), which apparently contradicts to the broadband conduction mechanism [19]. On the other hand, the thermopower variations can be described by a simplified model neglecting transported heat of the holes [19,29]

$$\alpha = (1 - t_0) \frac{k}{e} \left(\ln \frac{N}{[h]} \right) + t_0 \left(-\frac{k}{4e} \ln p(\text{O}_2) + \alpha_0^0 \right) \quad (1)$$

where N is the number of states, α_0^0 is a temperature-dependent constant, and the hole concentration $[h]$ related to one formula unit is determined from the oxygen non-stoichiometry data. The fitting results are shown in Fig. 3C as solid lines; Table 1 lists the regression parameters. One should mention that this model can be applied both for a broadband mechanism of the hole transport if the density of states is $p(\text{O}_2)$ -independent, and for polaron hopping if the charge-carrier concentration is relatively low compared to the number of available sites. In the latter case, the values of N close to 1/3 per formula unit (Table 1) would imply significant site-exclusion effects near Ni^{3+} and/or Fe^{3+} , in agreement with the $p(\text{O}_2)$ - T - δ diagram modelling results [11]. No unambiguous conclusion on the conduction mechanism may hence be drawn on the basis of thermopower data.

Moreover, the hole mobility in $\text{La}_2\text{Ni}_{0.9}\text{Fe}_{0.1}\text{O}_{4+\delta}$ is close to the characteristic threshold of $0.1 \text{ cm}^2 \text{ V}^{-1} \text{ s}^{-1}$, considered to separate small-polaron and broadband conduction (Fig. 4B). Transitions from itinerant to localized electronic behavior are often observed

Table 1
Fitting parameters of the $p(\text{O}_2)$ -dependencies of Seebeck coefficient of $\text{La}_2\text{Ni}_{0.9}\text{Fe}_{0.1}\text{O}_{4+\delta}$ at $p(\text{O}_2) = 5 \times 10^{-5}$ – 0.45 atm using Eq. (1) as regression model

T (K)	N	$-\alpha_0^0$ (mV K^{-1})
1073	0.350 ± 0.007	53 ± 2
1123	0.326 ± 0.005	16.6 ± 0.6
1173	0.312 ± 0.005	3.1 ± 0.1
1223	0.316 ± 0.008	2.3 ± 0.2

in perovskite-like $(\text{La,Sr})\text{MO}_{3-\delta}$ ($M = \text{Fe, Co, Ni}$) phases [30,31] and may be caused by numerous factors, particularly doping and changes in the oxygen chemical potential. For $(\text{La,Sr})\text{CoO}_{3-\delta}$ perovskites, the oxygen deficiency variations under oxidizing conditions can be described using the electron-gas rigid-band model [19]; the non-stoichiometry and electrical properties of $(\text{La,Sr})\text{FeO}_{3-\delta}$ exhibit tendencies typical for both itinerant and localized behavior [25]. In order to clarify the defect-formation and transport mechanisms in lanthanum nickelate-based phases, validity of the rigid-band model was examined by re-analyzing the $p(\text{O}_2)$ - T - δ diagrams of $\text{La}_2\text{Ni}_{0.9}\text{Fe}_{0.1}\text{O}_{4+\delta}$ and $\text{La}_2\text{NiO}_{4+\delta}$.

3.2. Oxygen intercalation

The statistical-thermodynamic models describing oxygen non-stoichiometry in La_2NiO_4 -based phases, which take into account the point-defect interaction and site-exclusion effects, were reported in previous works [11,15]. Briefly, these models are based on the discrete Fermi–Dirac distribution and the general equation for the defect chemical potential (μ):

$$\begin{aligned} \mu(\text{Df}_X^z) &= \mu^0(\text{Df}_X^z) + RT \ln a(\text{Df}_X^z) \\ &= \mu^0(\text{Df}_X^z) + RT \ln \frac{[\text{Df}_X^z]}{N(\text{Df}_X^z) - [\text{Df}_X^z]} \end{aligned} \quad (2)$$

where $[\text{Df}_X^z]$ is the concentration of defects Df_X^z in the X sublattice, z is their charge, $N(\text{Df}_X^z)$ is the number of states, and a is the activity. The discrete density of states can be assessed statistically by analyzing the probability (P) of different defect configurations for a fixed overall composition via the binomial distribution:

$$P(\text{Df}_X^z, \text{Nh}_Y^w, m) = \binom{n_{YX}}{m} \left(\frac{[\text{Nh}_Y^w]}{[Y_{\text{max}}]} \right)^m \left(1 - \frac{[\text{Nh}_Y^w]}{[Y_{\text{max}}]} \right)^{n_{YX}-m} \quad (3)$$

where Nh_Y^w is a lattice element introduced in the same or other sublattice (Y) and affecting $\mu(\text{Df}_X^z)$, n_{YX} is the number of Y sites neighboring the given X position, w is the charge of Nh_Y^w species, m is their number in the X neighborhood, $\binom{n_{YX}}{m}$ is the binomial coefficient, and $[Y_{\text{max}}]$ is the number of Y sites per formula unit. The total number of states at a k th level may be calculated as the product of partial probabilities multiplied by the total concentration of sites where the given defects can be located. The general equation used to analyze the relationships between concentrations and activities of mobile defects, namely holes and oxygen interstitials O_i^{2-} , is thus written as

$$\begin{aligned} [\text{Df}_X^z] &= \sum_{k=0}^{r_k} \frac{N(\text{Df}_X^z, k)}{\exp[E_k/RT - \ln a(\text{Df}_X^z)] + 1} \\ &= a(\text{Df}_X^z) \sum_{k=0}^{r_k} \frac{N(\text{Df}_X^z, k)}{\exp[E_k/RT] + a(\text{Df}_X^z)} \end{aligned} \quad (4)$$

where r_k is the total number of energy levels and E_k is the energy of k th level given with respect to the ground level. Due to strong coulombic repulsion between the oxygen interstitial anions, their location in nearest-neighboring positions is excluded, resulting in

$m = 0$ and

$$N(O_i^{2-}) = [O_{iMax}]P(O_i^{2-}, O_i^{2-}, n_{O_i}, 0) \quad (5)$$

where $[O_{iMax}] = 4$ is the number of interstitial sites per formula unit. Similar limitations exist also in the case of p-type electronic charge carriers, when the activity depends on the presence of other defects in the second coordination sphere and the total concentration is determined by the crystal electroneutrality condition [11,15].

The rigid-band approximation is based on a general assumption that the bandgap variations induced by guest atom incorporation occur without essential alterations in the energy dependence of the density of states, $g(E)$, in the conduction and valence bands [20,21]. This means, in particular, that the bands remain perfectly rigid on doping. In framework of the electron-gas rigid-band model simplified according to Ref. [19], the total number of conduction electrons per formula unit, $[e]$, may be evaluated by integrating the product of Fermi–Dirac distribution function, $f(E)$, and density of states over the whole bandwidth and neglecting the electron entropy:

$$[e] = \int_{E_b}^{E_t} g(E)f(E) dE \approx \int_{E_b}^{E_F} g(E) dE \quad (6)$$

where E_F is the Fermi level, and E_b and E_t are the energies at the band bottom and top, correspondingly. Using the first-order Taylor expansion of Eq. (6) in accordance with Ref. [19], the hole chemical potential can be expressed as

$$\mu = \mu(h^0) + \frac{[h] - [h^0]}{g(\mu)} \quad (7)$$

where $g(\mu)$ is the electronic density of states at the Fermi level, and $[h^0]$ is the hole concentration in the state when the average oxidation state of nickel cations is +2. This formalism implies that increasing hole population due to any increase of the oxygen excess shifts only the Fermi level and has no effect on other energetic parameters of the electronic sublattice, which may influence oxygen intercalation. Another necessary comment is that the rigid-band approach discards specific interactions, such as screening, electron-correlation or exchange phenomena [19]; this may lead to serious limitations for the description of complex oxides electronic structure [21]. Whatever the model limitations, the chemical potential of oxygen interstitials can still be expressed by Eqs. (2)–(5), because the formation processes of oxygen interstitial anions and holes occur in the different layers of K_2NiF_4 -type lattice and the interaction of ionic and electronic charge carriers may thus be neglected.

Fig. 5 and Table 2 compare the fitting results for $La_2NiO_{4+\delta}$ and $La_2Ni_{0.9}Fe_{0.1}O_{4+\delta}$. Although both models provide an adequate description of the oxygen non-stoichiometry variations with temperature and oxygen partial pressure, the site-exclusion approach seems more appropriate for the iron-substituted nickelate. The reverse situation is observed for undoped $La_2NiO_{4+\delta}$. Therefore, as for numerous perovskite-like systems (e.g. [19,30,31] and references therein), doping with iron promotes hole localization in the K_2NiF_4 -type lanthanum nickelate. Most likely, this effect is primarily associated with the formation of stable Fe^{3+} states as confirmed by the Mössbauer spectroscopy [11].

3.3. Surface-limited oxygen transport

Fig. 6 displays the steady-state oxygen permeation fluxes (j) through dense $La_2Ni_{0.9}Fe_{0.1}O_{4+\delta}$ membranes of different thickness, and the specific permeability $J(O_2)$ calculated

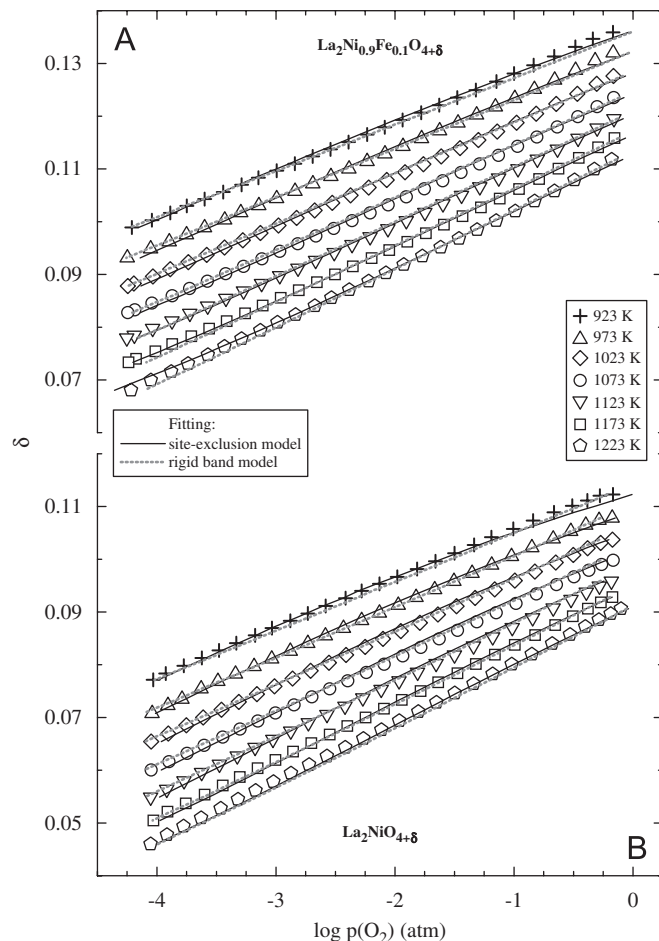


Fig. 5. The $p(O_2)$ – T – δ diagrams of $La_2Ni_{0.9}Fe_{0.1}O_{4+\delta}$ (A) and $La_2NiO_{4+\delta}$ (B). Solid and dashed lines correspond to the fitting results using site-exclusion and rigid-band models, respectively.

as [4,18]

$$J(O_2) = jL_m \left(\ln \frac{p_2}{p_1} \right)^{-1} \quad (8)$$

where L_m is the membrane thickness and p_1 is the permeate-side oxygen pressure. Increasing L_m leads to lower oxygen fluxes, whereas the specific permeability proportional to $j \times L_m$ increases with membrane thickness due to a decreasing role of the surface exchange processes. This indicates that both bulk ionic conduction and surface exchange kinetics have non-negligible effects on the overall oxygen transport.

In light of this, the experimental data of oxygen permeation fluxes were modelled splitting the overall oxygen chemical potential gradient across $La_2Ni_{0.9}Fe_{0.1}O_{4+\delta}$ membranes into three parts, which correspond to the membrane bulk ($\Delta\mu^{bulk}$), the permeate-side ($\Delta\mu_1^{surf}$) and feed-side ($\Delta\mu_2^{surf}$) surfaces. The bulk contribution is determined by the partial ionic and electronic conductivities according to the Wagner equation:

$$\begin{aligned} j &= \frac{1}{16F^2 L_m} \int_{\mu_1^{surf}}^{\mu_2^{surf}} \frac{\sigma_O \sigma_h}{\sigma_O + \sigma_h} d\mu(O_2) \\ &= \frac{RT}{16F^2 L_m} \int_{\ln p_1^s}^{\ln p_2^s} \sigma_O \left(1 - \frac{\sigma_O}{\sigma} \right) d \ln p(O_2) \end{aligned} \quad (9)$$

where p_1^s and p_2^s are the $p(O_2)$ values at the permeate- and feed-side surfaces, respectively. The ionic conductivity is defined

Table 2
Parameters of the regression models for $p(\text{O}_2)$ - T - δ diagrams of $\text{La}_2\text{NiO}_{4+\delta}$ -based phases

Fitting parameters	Site-exclusion model		Rigid band model	
	$\text{La}_2\text{Ni}_{0.9}\text{Fe}_{0.1}\text{O}_{4+\delta}$	$\text{La}_2\text{NiO}_{4+\delta}$	$\text{La}_2\text{Ni}_{0.9}\text{Fe}_{0.1}\text{O}_{4+\delta}$	$\text{La}_2\text{NiO}_{4+\delta}$
$(\Delta H_{\text{ex}} - 1/2H_{\text{O}_2}^0)$ (kJ mol ⁻¹)	103 ± 1	94 ± 1	139 ± 1	155 ± 2
$(\Delta S_{\text{ex}} - 1/2S_{\text{O}_2}^0)$ (J mol ⁻¹ K ⁻¹)	-3 ± 1	-12 ± 1	-20 ± 1	-20 ± 1
$\Delta E_{\text{h} \rightarrow \text{h}}$ (kJ mol ⁻¹)	13.0 ± 0.2	11.2 ± 0.3	-	-
ΔH_{ion} (kJ mol ⁻¹)	47 ± 2	-	-	-
$g[\mu(h^0)] \times 10^6$ (J ⁻¹ mol)	-	-	4.34 ± 0.03	4.67 ± 0.04
Adjusted correlation coefficient	0.999	0.998	0.999	0.999
Relative error (%)	1.0	1.3	1.1	1.0

Notes: $(\Delta H_{\text{ex}} - 1/2H_{\text{O}_2}^0)$ and $(\Delta S_{\text{ex}} - 1/2S_{\text{O}_2}^0)$ are the enthalpy and entropy for oxygen de-intercalation, corrected for the standard thermodynamic functions of gaseous molecular oxygen (see Ref. [15]).

$\Delta E_{\text{h} \rightarrow \text{h}}$ and ΔH_{ion} are the hole interaction energy and enthalpy of the reaction $\text{Fe}^{3+} + \text{Ni}^{2+} \leftrightarrow \text{Fe}^{2+} + \text{Ni}^{3+}$ [11].

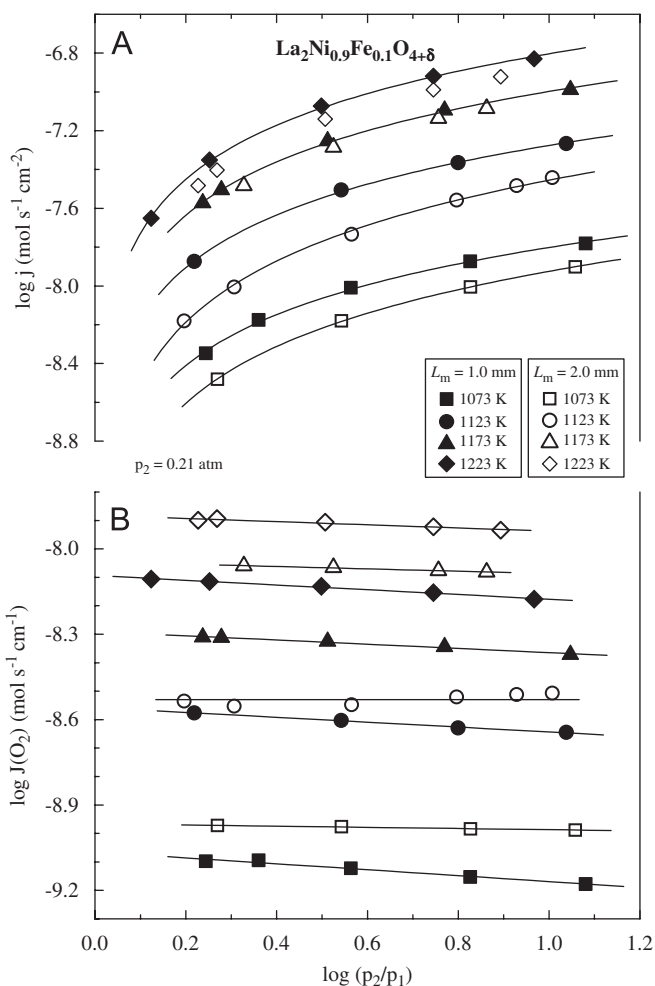


Fig. 6. Dependence of the oxygen permeation fluxes (A) and specific oxygen permeability (B) of dense $\text{La}_2\text{Ni}_{0.9}\text{Fe}_{0.1}\text{O}_{4+\delta}$ membranes on the oxygen partial pressure gradient.

as [32]:

$$\sigma_0 = 2eu_0[\text{O}_i^{2-}]Z_{\text{fu}}/V_{\text{uc}} \quad (10)$$

where $[\text{O}_i^{2-}]$ is the concentration of oxygen interstitials per unit formula, Z_{fu} is the number of formula units per unit cell, V_{uc} is the unit cell volume calculated from XRD results, and u_0 is the anion mobility independent of the oxygen non-stoichiometry. The latter assumption was based on the structural and thermodynamic data

Table 3
Parameters of the regression models for oxygen permeation through dense $\text{La}_2\text{Ni}_{0.9}\text{Fe}_{0.1}\text{O}_{4+\delta}$ membranes^a

T (K)	J^0 (nmol s ⁻¹ cm ⁻²)	$u_0 \times 10^4$ (cm V ⁻¹ s ⁻¹)	n^b	R_{adj}^c
1223	260 ± 10	13 ± 1	1	0.999
1173	160 ± 10	12 ± 3		0.993
1123	130 ± 20	1.8 ± 0.1		0.996
1073	31 ± 1	0.77 ± 0.03		0.999
1223	190 ± 10	9 ± 2	2	0.992
1173	123 ± 9	7 ± 2		0.98
1123	90 ± 10	1.7 ± 0.1		0.996
1073	22 ± 1	0.67 ± 0.05		0.997
1223	159 ± 8	6.8 ± 0.9	4	0.98
1173	108 ± 5	5.1 ± 0.9		0.95
1123	65 ± 6	1.57 ± 0.09		0.994
1073	18 ± 1	0.56 ± 0.03		0.99

^a $L_m = 1.0$ – 2.0 mm.

^b Data for fixed n values are given.

^c R_{adj} is the adjusted correlation coefficient.

([13–16] and references cited), which reveal that the number of interstitial positions in $\text{La}_2\text{NiO}_{4+\delta}$ is substantially larger with respect to oxygen hyperstoichiometry under ambient conditions. The oxygen transfer through membrane/gas interfaces was expressed using a classical non-equilibrium thermodynamic expression [33]:

$$j = J^0 \left(1 - \exp \left[\frac{\Delta \mu_i^{\text{surf}}}{nRT} \right] \right) \quad (11)$$

where J^0 corresponds to the equilibrium exchange rate, and n is the stoichiometric coefficient showing the ratio between the fluxes of molecular O_2 and species involved in the rate-determining step. This formula represents a simplified solution of the model [34] proposed for oxygen exchange between a mixed conductor and the gas phase, and is qualitatively similar to the equation for solid-electrolyte cells where increasing electrode polarization leads to limiting currents [35]. In the latter case, the physical meaning of J^0 relates to the limiting flux of electrochemically active species, which may be governed by diffusion, adsorption or chemical reaction steps [35]. In the course of fitting the oxygen permeation data, Eqs. (9–11) were solved numerically; the relationships between $[\text{O}_i^{2-}]$ and oxygen chemical potential were described using the equilibrium $p(\text{O}_2)$ - T - δ diagram (Fig. 5A).

The results of regression analysis are summarized in Table 3; Fig. 7 shows one example of the simulated oxygen fluxes at 1223 K. As expected, decreasing membrane thickness leads to a

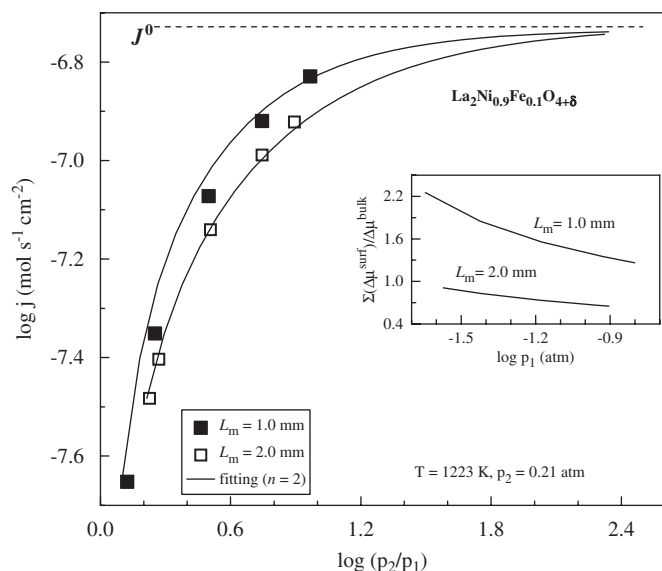


Fig. 7. One example of the fitting results of oxygen permeation fluxes through $\text{La}_2\text{Ni}_{0.9}\text{Fe}_{0.1}\text{O}_{4+\delta}$ membranes at 1223 K. Inset shows the ratio between the oxygen chemical potential drops at the membrane surfaces and in the bulk, plotted vs. permeate-side oxygen pressure.

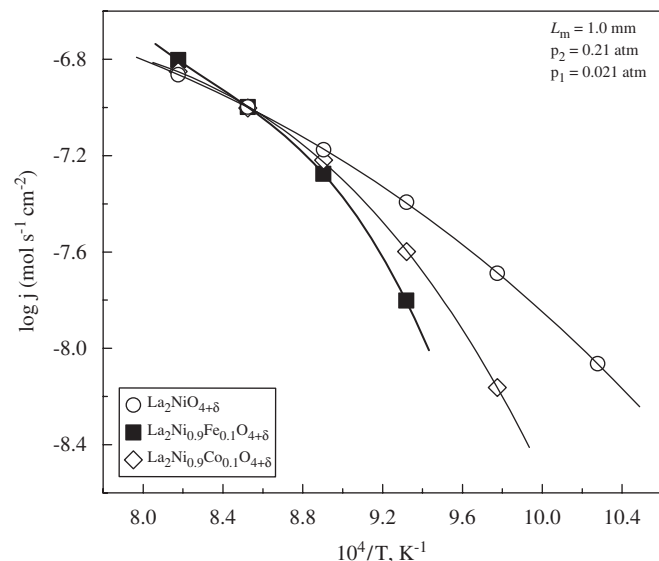


Fig. 8. Temperature dependence of the oxygen permeation flux through $\text{La}_2\text{Ni}_{0.9}\text{Fe}_{0.1}\text{O}_{4+\delta}$ ceramics under fixed $p(\text{O}_2)$ gradient, compared to the data on $\text{La}_2\text{NiO}_{4+\delta}$ [23] and $\text{La}_2\text{Ni}_{0.9}\text{Co}_{0.1}\text{O}_{4+\delta}$ [27].

greater influence of the surface exchange kinetics (inset in Fig. 7). The best fitting quality was obtained by fixing the n value equal to 1 or 2; introducing n as a regression parameter caused statistical degeneration of the model. At the same time, applying this model to undoped $\text{La}_2\text{NiO}_{4+\delta}$ resulted in $n = 2$ [23]. As $\text{La}_2\text{NiO}_{4+\delta}$ and $\text{La}_2\text{Ni}_{0.9}\text{Fe}_{0.1}\text{O}_{4+\delta}$ membranes exhibit quite similar behavior and comparable oxygen fluxes (Fig. 8), analogous permeation mechanisms are expected for both these materials. The authors [34] suggested that for oxygen-deficient mixed conductors, the situation with $n = 1$ corresponds to rate-limiting oxygen adsorption or dissociation, while $n = 2$ indicates slow incorporation of the surface oxygen vacancies into the lattice bulk. In the case of the K_2NiF_4 -type compounds, the oxygen vacancies formed in the perovskite-like layers due to intrinsic Frenkel disordering may

also act as the active surface sites for oxygen adsorption. One may assume, therefore, that the rate-determining step of oxygen surface exchange may involve species related to one oxygen atom, anion or site participating in the reaction. The tendency to limiting fluxes may appear due to stagnated surface migration of such species, or to a slow vacancy formation and/or diffusion from/into the membrane bulk. The discharge processes should be fast since the electronic conductivity of La_2NiO_4 -based phases is much higher than ionic (Fig. 4). Since the content of hyperstoichiometric oxygen is low with respect to the concentration of interstitial positions, the latter factor cannot be critical as well.

Irrespective of the microscopic mechanisms, the surface exchange limitations increase with increasing oxygen partial pressure gradient (Fig. 7). When the p_2/p_1 ratio becomes higher than 100, the calculated oxygen fluxes tend to approach J^0 . This type of behavior is responsible for the stable operation of La_2NiO_4 -based membranes under high oxygen chemical potentials gradients, such as air/ CH_4 [5,12]. The apparent activation energy (E_a) for oxygen permeation through $\text{La}_2\text{Ni}_{0.9}\text{Fe}_{0.1}\text{O}_{4+\delta}$ decreases on heating, but is substantially higher than that for the oxygen ionic conductivity and mobility. For comparison, in the case of one $\text{La}_2\text{Ni}_{0.9}\text{Fe}_{0.1}\text{O}_{4+\delta}$ membrane with $L_m = 1.0$ mm at temperatures above 1123 K, the oxygen permeability activation energy is 124 kJ mol^{-1} ; the E_a values for the calculated ion mobility and conductivity are $69\text{--}70 \text{ kJ mol}^{-1}$.

3.4. Catalytic behavior

The CH_4 -TPR tests demonstrated that at temperatures below 970 K the rate of dry methane oxidation by the lattice oxygen of $\text{La}_2\text{Ni}_{0.9}\text{Fe}_{0.1}\text{O}_{4+\delta}$ is very low (Figs. 9 and 10). On heating up to 1030–1070 K, a drastic increase in the CH_4 conversion rate is observed. Initially this process is characterized by significant CO_2 yields indicative of total combustion. Further heating leads to a

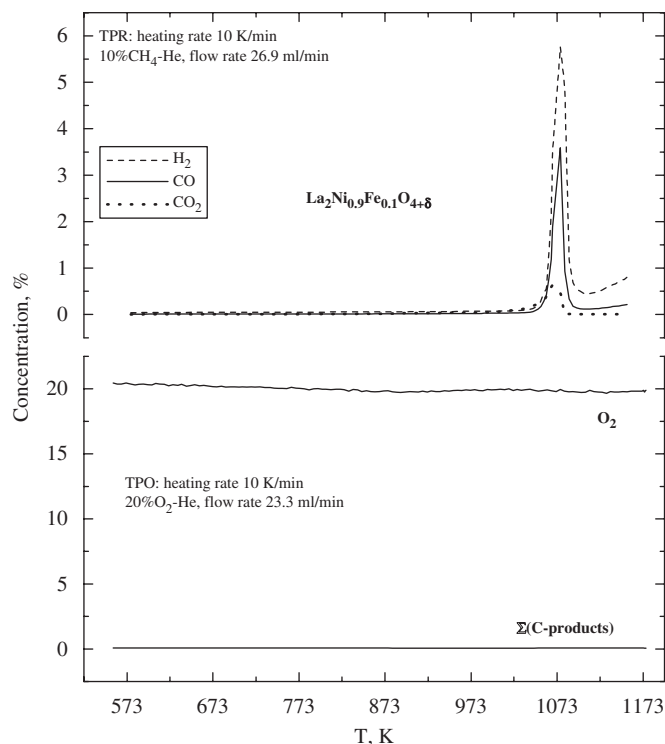


Fig. 9. Typical examples of the CH_4 -TPR (top) and TPO (bottom) data, illustrating catalytic behavior of $\text{La}_2\text{Ni}_{0.9}\text{Fe}_{0.1}\text{O}_{4+\delta}$. $\Sigma(\text{C-products})$ denotes the sum of all C-containing components.

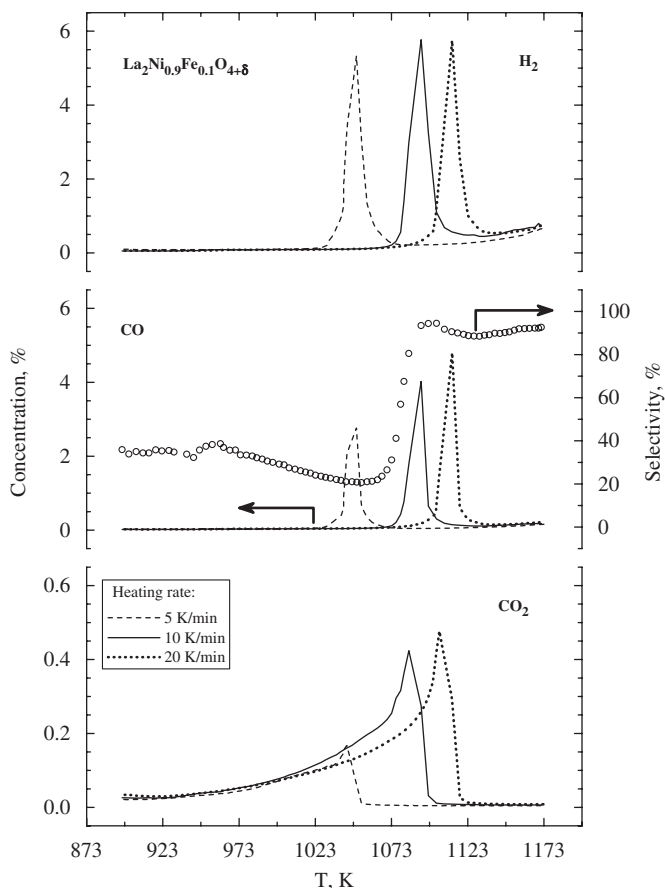


Fig. 10. H₂, CO and CO₂ concentrations in the effluent gas mixture during CH₄-TPR tests performed with different heating rates, and the CO selectivity calculated for the heating rate of 10 K min⁻¹.

dominant role of the partial oxidation of methane (POM), yielding CO and H₂; the selectivity to carbon monoxide formation achieves 90–95%. This behavior exhibits an excellent reproducibility irrespective of the heating rate, which only shifts the temperature corresponding to maximum CH₄ conversion. Furthermore, no substantial degradation in the catalytic activity was revealed in the course of redox cycling. Such properties may be advantageous for the ceramic membrane reactors.

In order to identify key factors relevant to the high catalytic activity, a series of TGA experiments were performed under non-equilibrium conditions similar to the CH₄-TPR tests, in a 10% H₂–90% N₂ flow (Fig. 11). Comparison of the non-equilibrium TGA and CH₄-TPR data and the equilibrium coulometric titration results unambiguously showed that, under conditions where the catalytic activity starts to increase, the total oxygen content becomes lower than minimum (4+ δ) values in the K₂NiF₄-type phase. For instance, reversible decrease of the oxygen partial pressure in the coulometric titration cell down to approximately 5×10^{-13} atm at 1223 K results in La₂Ni_{0.9}Fe_{0.1}O_{4+ δ} decomposition, reflected by a stepwise decrease in the oxygen content and confirmed by XRD. The minimum oxygen content in K₂NiF₄-type phase at 1223 K was determined as 4.011–4.012 atoms per formula unit, suggesting that a significant part of iron cations remains trivalent on decomposition; the low- $p(\text{O}_2)$ stability boundary of La₂Ni_{0.9}Fe_{0.1}O_{4+ δ} (Table 4) is close to that of parent La₂NiO_{4+ δ} [16,36]. XRD analysis demonstrated that the decomposition occurs via the separation of metallic nickel and lanthanum oxide, as for undoped lanthanum nickelate [36]. Since

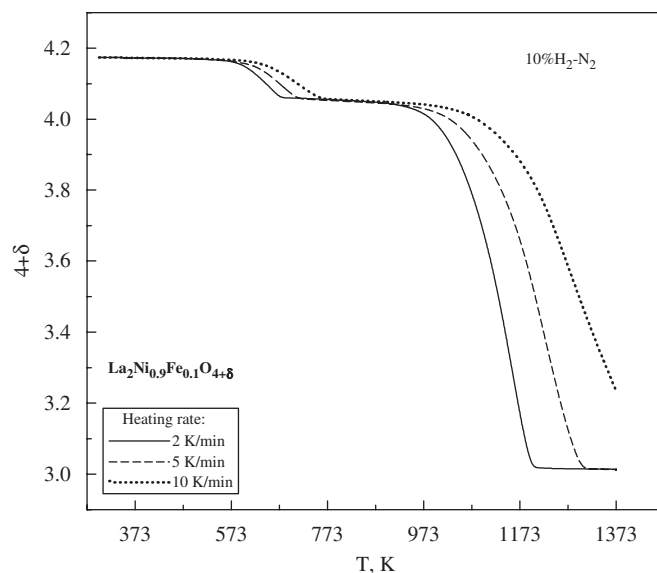


Fig. 11. Non-equilibrium oxygen content in La₂Ni_{0.9}Fe_{0.1}O_{4+ δ} measured by TGA on heating in flowing 90% H₂–90% N₂ gas mixture.

Table 4

Approximate low- $p(\text{O}_2)$ stability limits of La₂NiO₄-based phases at 1223 K

Composition	$p(\text{O}_2)$ (atm)	Method	Reference
La ₂ Ni _{0.9} Fe _{0.1} O _{4+δ}	5×10^{-13}	Coulometric titration	This work
La ₂ Ni _{0.8} Cu _{0.2} O _{4+δ}	2×10^{-13}	Conductivity and thermopower measurements vs. $p(\text{O}_2)$	[27]
La ₂ NiO _{4+δ}	6×10^{-14}	XRD after annealing at various $p(\text{O}_2)$	[16]
	6×10^{-13}	Electromotive force measurements of solid-electrolyte cells	[36]

the maximum CO and H₂ yields are observed in conditions when the total oxygen content in La₂Ni_{0.9}Fe_{0.1}O_{4+ δ} becomes lower than 4 atoms per unit formula (Figs. 9–11), the high activity towards POM can be undoubtedly attributed to the segregation of metallic nickel. This explains the predominant role of the total combustion mechanism in the case of dry CH₄ oxidation over planar La₂NiO₄-based membranes where no decomposition occurs due to surface-limited oxygen transport [12,18].

4. Conclusions

The combined analysis of oxygen non-stoichiometry, total conductivity, Seebeck coefficient, oxygen permeability and catalytic behavior of La₂Ni_{0.9}Fe_{0.1}O_{4+ δ} has made it possible to clarify several mechanisms relevant to potential applications of lanthanum nickelate-based materials in high-temperature electrochemical devices. Under oxidizing conditions, the dominating electronic conduction in La₂Ni(Fe)O_{4+ δ} is governed by the p-type charge carriers, which are essentially localized on nickel cations. While the electrical properties exhibit trends typical for both itinerant and polaron hopping behavior, the incorporation of iron

cations promotes hole localization and decreases conductivity. In contrast, the hole chemical potential variations in undoped $\text{La}_2\text{NiO}_{4+\delta}$ can be described by the electron-gas rigid-band model. Reducing oxygen chemical potential leads to decomposition of $\text{La}_2\text{Ni}_{0.9}\text{Fe}_{0.1}\text{O}_{4+\delta}$, which occurs close to the low- $p(\text{O}_2)$ stability boundary of undoped lanthanum nickelate; the resultant segregation of metallic Ni is responsible for high catalytic activity towards the partial oxidation of methane at temperatures above 1000–1050 K. The surface-limited oxygen permeation through dense $\text{La}_2\text{Ni}_{0.9}\text{Fe}_{0.1}\text{O}_{4+\delta}$ membranes is adequately described within the framework of non-equilibrium thermodynamics, assuming that the bulk ionic conductivity is proportional to the oxygen interstitials concentration.

Acknowledgments

This work was partially supported by the FCT, Portugal (Projects POCI/CTM/59197/2004, PTDC/CTM/64357/2006, and SFRH/BPD/28629/2006). Experimental assistance and helpful discussions made by A. Yaremchenko, A. Shaula and Y. Pivak, are gratefully acknowledged.

References

- [1] B. Vigeland, R. Glenne, T. Breivik, S. Julsrud, Int. Patent Application PCT WO 99/59702, 1999.
- [2] J.A. Kilner, C.K.M. Shaw, Solid State Ionics 154–155 (2002) 523.
- [3] V.V. Vashook, I.I. Yushkevich, L.V. Kokhanovsky, L.V. Makhnach, S.P. Tolochko, I.F. Kononyuk, H. Ullmann, H. Altenburg, Solid State Ionics 119 (1999) 23.
- [4] V.V. Kharton, A.P. Viskup, E.N. Naumovich, F.M.B. Marques, J. Mater. Chem. 9 (1999) 2623.
- [5] D.C. Zhu, X.Y. Xu, S.J. Feng, W. Liu, C.S. Chen, Catal. Today 82 (2003) 151.
- [6] M. Al Daroukh, V.V. Vashook, H. Ullmann, F. Tietz, I. Arual Raj, Solid State Ionics 158 (2003) 141.
- [7] C.N. Munnings, S.J. Skinner, G. Amow, P.S. Whitfield, I.J. Davidson, Solid State Ionics 176 (2005) 1895.
- [8] E. Boehm, J.-M. Bassat, P. Dordor, F. Mauvy, J.-C. Grenier, Ph. Stevens, Solid State Ionics 176 (2005) 2717.
- [9] S. Miyoshi, T. Furuno, H. Matsumoto, T. Ishihara, Solid State Ionics 177 (2006) 2269.
- [10] A.V. Kovalevsky, V.V. Kharton, A.A. Yaremchenko, Y.V. Pivak, E.V. Tsipis, S.O. Yakovlev, A.A. Markov, E.N. Naumovich, J.R. Frade, J. Electroceram. 18 (2007) 205.
- [11] E.V. Tsipis, E.N. Naumovich, M.V. Patrakeev, J.C. Waerenborgh, Y.V. Pivak, P. Gaczyński, V.V. Kharton, J. Phys. Chem. Solids 68 (2007) 1443.
- [12] V.V. Kharton, A.A. Yaremchenko, A.A. Valente, V.A. Sobyenin, V.D. Belyaev, G.L. Semin, S.A. Veniaminov, E.V. Tsipis, A.L. Shaula, J.R. Frade, J. Rocha, Solid State Ionics 176 (2005) 781.
- [13] J.D. Jorgensen, B. Dabrowski, S. Pei, D.R. Richards, D.G. Hinks, Phys. Rev. B 40 (1989) 2187.
- [14] A. Demourgues, A. Wattiaux, J.C. Grenier, M. Pouchard, J.L. Soubeyroux, J.M. Dance, P. Hagenmuller, J. Solid State Chem. 105 (1993) 458.
- [15] E.N. Naumovich, M.V. Patrakeev, V.V. Kharton, A.A. Yaremchenko, D.I. Logvinovich, F.M.B. Marques, Solid State Sci. 7 (2005) 1353.
- [16] D.E. Rice, D.J. Buttrey, J. Solid State Chem. 105 (1993) 197.
- [17] F. Mauvy, E. Boehm, J.M. Bassat, J.C. Grenier, J. Fouletier, Solid State Ionics 178 (2007) 1200.
- [18] V.V. Kharton, A.A. Yaremchenko, E.V. Tsipis, A.A. Valente, M.V. Patrakeev, A.L. Shaula, J.R. Frade, J. Rocha, Appl. Catal. A 261 (2004) 25.
- [19] M.H.R. Lankhorst, PhD Thesis, 1997. University of Twente, Enschede.
- [20] S. Raimes, J. Phys. 23 (1962) 639.
- [21] K. Horiba, A. Chikamatsu, H. Kumigashira, M. Oshima, N. Nakagawa, M. Lippmaa, K. Ono, M. Kawasaki, H. Koinuma, Phys. Rev. B 71 (2005) 155420.
- [22] E.V. Tsipis, V.V. Kharton, J.R. Frade, Electrochim. Acta 52 (2007) 4428.
- [23] E.V. Tsipis, E.N. Naumovich, A.L. Shaula, M.V. Patrakeev, J.C. Waerenborgh, V.V. Kharton, Solid State Ionics 179 (2008) 57.
- [24] L.A. Chick, L. Pederson, G.D. Maupin, J.L. Bates, L.E. Thomas, G.L. Exarhos, Mater. Lett. 10 (1990) 6.
- [25] M.V. Patrakeev, E.B. Mitberg, A.A. Lakhtin, I.A. Leonidov, V.L. Kozhevnikov, V.V. Kharton, M. Avdeev, F.M.B. Marques, J. Solid State Chem. 167 (2002) 203.
- [26] F.M.B. Marques, G.P. Wirtz, J. Am. Ceram. Soc. 75 (1992) 369.
- [27] V.V. Kharton, A.A. Yaremchenko, A.L. Shaula, M.V. Patrakeev, E.N. Naumovich, D.I. Logvinovich, J.R. Frade, F.M.B. Marques, J. Solid State Chem. 177 (2004) 26.
- [28] J.B. Goodenough, in: N. Klein, D.S. Tannhauser, M. Pollak (Eds.), Conduction in Low-Mobility Materials, Taylor & Francis, London, 1971, p. 87.
- [29] S. Yamaguchi, K. Kobayashi, T. Higuchi, S. Shin, Y. Iguchi, Solid State Ionics 136 (2000) 305.
- [30] J.B. Goodenough, J.-S. Zhou, in: J.B. Goodenough (Ed.), Localized to Itinerant Electronic Transition in Perovskite Oxides, Springer, Berlin, Heidelberg, 2001, p. 17.
- [31] J. Mizusaki, Solid State Ionics 52 (1992) 79.
- [32] P. Kofstad, Nonstoichiometry, Diffusion and Electrical Conductivity in Binary Metal Oxides, Wiley, New York, 1972.
- [33] S.R. de Groot, P. Mazur, Nonequilibrium Thermodynamics, Dover, New York, 1984.
- [34] S.B. Adler, X.Y. Chen, J.R. Wilson, J. Catal. 245 (2007) 91.
- [35] V.N. Chebotin, M.V. Perfiliev, Electrochemistry of Solid Electrolytes, Technical Information Center, US Department of Energy, Oak Ridge, 1978.
- [36] V.A. Cherepanov, A.N. Petrov, L.Y. Grimova, E.M. Novitsky, Z. Fiz. Khim. 57 (1983) 859 (in Russian).